Journal of Applied Polymer Science

Herbally Derived Polymeric Nanofibrous Scaffolds for Bone Tissue Regeneration

S. Suganya,[1,2] Jayarama Venugopal,[3] Seeram Ramakrishna,[3] B. S. Lakshmi,[2] V. R. Giri Dev[1]

[1]Department of Textile Technology, Anna University, Chennai 600025, Tamil Nadu, India
[2]Centre for Biotechnology, Anna University, Chennai 600025, Tamil Nadu, India
[3]Center for Nanofibers and Nanotechnology, E3-05-14, Nanoscience and Nanotechnology Initiative, Faculty of Engineering, National University of Singapore, 2 Engineering Drive 3, Singapore 117576, Singapore
Correspondence to: V. R. Giri Dev (E-mail: vrgiridev@yahoo.com)

ABSTRACT: Hydroxyapatite (HA), the bone mineral and *Cissus quadrangularis* (CQ), a medicinal plant with osteogenic activity, are attaining increasing interest as a potential therapeutic agent for enhanced bone tissue regeneration. In the present study a synergistic effect of these two agents were analyzed by fabricating PCL-CQ-HA nanofibrous scaffolds by electrospinning and compared with PCL-CQ and PCL (control) nanofibrous scaffolds. Morphology, composition, hydrophilicity, and mechanical properties of the electrospun PCL, PCL-CQ, PCL-CQ-HA nanofibrous scaffolds were examined by Field emission scanning electron microscopy (FESEM), Fourier transform infrared spectroscopy (FTIR), Contact angle and Tensile tests, respectively. The response of human foetal osteoblast cells on these scaffolds were evaluated using MTS assay, alkaline phosphatase activity, alizarin red staining, and osteocalcin expression for bone tissue regeneration. While the observed cellular response to both groups of scaffolds was better than for the control PCL scaffold, the PCL-CQ-HA nanofibrous scaffolds provided the most favorable substrate for cell proliferation and mineralization. The results showed that PCL-CQ-HA nanofibrous scaffolds had appropriate surface roughness for the osteoblast adhesion, proliferation, and mineralization comparing with other scaffolds. The observed investigation of physicochemical and biological properties suggests that the CQ-HA loaded PCL nanofibrous scaffolds serve as a potential biocomposite material for bone tissue engineering. © 2013 Wiley Periodicals, Inc. J. Appl. Polym. Sci. **2014**, *131*, 39835.

KEYWORDS: biomaterials; biocompatibility; biomedical applications; bioengineering; biomimetic

Received 31 May 2013; accepted 8 August 2013
DOI: 10.1002/app.39835

INTRODUCTION

Tissue engineering is an emerging interdisciplinary field that applies the principles of biology and engineering to the development of viable substitutes that restore, maintain, and improve the function of human tissues.[1] It has the potential to produce immunologically tolerant "artificial" organ and tissue substitutes that can grow with the patient. This leads to a permanent solution to the damaged organ or tissue without the need for supplementary therapies, thus making it a cost-effective treatment in the long term chronic disease.[2] Cells, scaffolds, and growth-stimulating signals are generally referred as the tissue engineering triad, the key components of engineered tissues. Scaffolds provide the structural support for cell attachment and subsequent tissue development,[3] although various structures of engineered tissue scaffolds have been developed for tissue replacement, the ultimate goal of the scaffold design is the production of an ideal structure that can replace the natural ECM until host cells can repopulate and resynthesize a new natural matrix.[4] To achieve this goal, the scaffold material must be selected carefully and architecture must be designed to ensure that the seeded cells are biocompatible with the engineered nanofibrous scaffolds.

The scaffolds for bone tissue engineering should provide high structural integrity, high surface area for cell–material interaction and slow degradation at a rate which commensurate with the elucidation of new bone tissue formation.[5] Considerable efforts have attempted to develop scaffolds using biodegradable and biocompatible synthetic or natural polymers.[6] Polymeric scaffolds fabricated as nanosized fibers are well suited for bone tissue engineering as they can be shaped to fill anatomical defects; its architecture can be designed to provide the mechanical properties necessary to support cell growth, proliferation, differentiation, and motility; and it can be engineered to provide growth factors, drugs, therapeutics, and genes to stimulate tissue regeneration. Studies of cell-nanofiber

interactions have shown these cells adhere and proliferate well when cultured on polymeric nanofibrous scaffolds.[7–9]

Electrospun nanofibrous mats were fabricated from numerous synthetic and natural polymers such as poly(lactic acid) (PLA), poly(glycolic acid) (PGA), poly(ε-caprolactone) (PCL), poly(lactic-*co*-glycolic acid) (PLGA), proteins (e.g., collagen/gelatin) and polysaccharides (e.g., chitosan) that showed favorable results as scaffold for growing various kinds of cells. Nanofibrous membrane developed from poly(D, L-lactide-coglycolide) ultrafine fibers showed a morphological similarity to the ECM of natural tissue with a diameter ranging from 500 to 800 nm.[10] Synthetic polymers like PLGA and PLA-PEO copolymer encapsulated with DNA scaffolds were developed for therapeutic application in gene delivery for tissue engineering.[11] PCL/PVP nanofibrous mat containing herbal extracts from Tecomella undulata, exhibited antibacterial activity against pathogens.[12] Electrospun nonwoven PCL showed potential application as scaffold for bone tissue engineering.[13] Electrospun nanofibers with biologically significant polymers are of interest due to their potential biocompatibility and mechanical properties, but they do not possess the necessary bioactivity properties for tissue regeneration. In this perspective utilization of biologically active osteogenic agents are gaining much scrutiny of researchers. Electrospraying of hydroxyapatite (HA) nanoparticles onto the surface of polymer nanofibers provides a potentially novel substrate for the adhesion, proliferation and differentiation of mesenchymal stem cells (MSCs) into bone tissue regeneration.[14]

Plants have been used as a source of medicine throughout history and continue to serve as the basis for many pharmaceuticals used today. *Cissus quadrangularis* (CQ) is a medicinal plant possessing osteogenic activity and are attaining increasing interest as a potential therapeutic agent for enhancing bone healing.[15–18] The extracts of these plants are reported to contain phytoestrogenic steroids, ascorbic acid, flavonoids, carotene, and calcium.[19–21] Petroleum ether extract of CQ rich in phytosterol enhances bone marrow mesenchymal stem cell proliferation and foetal bone growth.[22] Several *in vivo* studies have demonstrated that CQ promotes ALP activity and enhances collagen synthesis in the fracture-healing process.[23] Polycaprolactone (PCL) and a potential polymers known for its biodegradable nature, chemical and thermal stability, good tissue compatibility, and solute permeability.[24,25] This viewpoint, we report here an herbal scaffolding approach for bone tissue engineering applications where the PCL-CQ-HA nanofibrous scaffolds were fabricated for bone tissue engineering. The study focused on assessing the impact of CQ compared with HA for cell growth, proliferation and mineralization for bone tissue regeneration.

MATERIALS AND METHODS

Preparation and Phytochemical Analysis of the Herbal Extract

Stem powder of *Cissus quadrangularis* (CQ) obtained from traditional herbal shop (Chennai, India) was used for the present study. About 50 g of CQ powder was soaked in 500 mL of 95% ethanol and kept in room temperature for 3 days in a static condition. Then the solution was filtered with crude filter paper followed by whatmann paper. Fine filtrate was subjected to rota evaporation after that 3 g of the material was obtained. The total ethanol extract was concentrated in a vacuum, dissolved in water, and then partitioned with petroleum ether to obtain a petroleum ether extract at a yield of 0.5 g. The obtained petroleum ether extract of CQ was subjected to "Salkowski test" to determine the presence of phytosterol, the main component responsible for osteoinductive property. In a test tube small quantity of extract was dissolved in 1 mL chloroform followed by the addition of few drops of concentrated sulphuric acid along the walls of the test tube. Formation of brown ring at the bottom of test tube indicates the presence of phytosterols.

Fabrication of Nanofibrous Scaffolds

PCL (Mw-80,000 g/mol) was purchased from Sigma-Aldrich (USA). CQ-loaded PCL solution was prepared by dissolving (5 wt %) of petroleum ether CQ extract in 10 mL of chloroform: methanol (4:1) followed by addition of PCL (10 wt %). PCL-CQ-HA solution was prepared by adding (10 wt %) of PCL, (5 wt %) of petroleum ether extract in 10 ml of chloroform: methanol (4:1) followed by addition of 4% nanosized hydroxyapatite particles. The PCL scaffold was prepared by adding 10 wt% of PCL in 10 mL of chloroform: methanol (4:1) which serves as a control. Prior to electrospinning, the solutions were stirred for 2 h. The solutions were then fed into a 3 mL standard syringe attached to a 21G blunted stainless steel needle respectively using a syringe pump (KDS 100, KD Scientific, Holliston, MA) at a flow rate of 1 mL/h with an applied voltage of 12 kV for all solutions (Gamma High Voltage Research, USA). On application of high voltage the polymer solution was drawn into fibers. Random fibers were collected on a flat collector plate wrapped with aluminum foil that was kept at a distance of 12 cm from the needle tip for characterization and were also collected on 15 mm cover slips by spreading them on the collector plate for cell culture studies.

Characterization of Nanofibrous Scaffolds

The surface morphology of electrospun nanofibrous scaffolds were studied under field emission scanning electron microscopy (FEI-QUANTA 200F, Netherland) at an accelerating voltage of 10 kV, after sputter coating with gold (JEOL JFC-1200 fine coater, Japan). Diameters of the electrospun fibers were analyzed from the SEM images using image analysis software (ImageJ, National Institutes of Health, USA). Hydrophilic nature of the electrospun nanofibrous scaffolds were measured by sessile drop water contact angle measurement using a VCA Optima Surface Analysis system (AST products, Billerica, MA). Distilled water was used for drop formation. The measured contact angle values reflected the hydrophilicity of the scaffolds. Tensile properties of electrospun nanofibrous scaffolds were determined with a tabletop tensile tester (Instron 3345, USA) using load cell of 10 N capacities. Rectangular specimens of dimensions 10 x 20 mm were used for testing, at a cross-head speed of 10 mm/min and the data was recorded for every 50 microseconds. The room conditions were controlled at 25°C and 34% humidity. Tensile stress–strain and

elastic modulus were calculated based on the generated tensile stress–strain curve. FTIR spectroscopic analysis of electrospun nanofibrous scaffolds was performed on Avatar 380, Thermo Nicolet, Waltham, MA) over a range of 500–4000 cm^{-1} at a resolution of 2 cm^{-1}.

Human Fetal Osteoblast (hFOB)

hFOB cells were cultured in DMEM/F12 media (1:1) supplemented with 10% foetal bovine serum and 1% antibiotic and antimycotic solutions (Invitrogen Corp, USA) in a 75 cm^2 cell culture flask. Cells were incubated at 37°C in a humidified atmosphere containing 5% CO_2 for 6 days and the culture medium was changed once in every 3 days. hFOB were harvested from 3rd passage cultures by trypsin EDTA treatment and replated. Populations of cell lines used in this study were between passage 3 and 4. Each of the nanofibrous scaffolds on 15 mm cover slip was placed in 24-well plate and pressed with a stainless steel ring to ensure complete contact of the scaffolds. The specimens were sterilized under UV light, washed thrice with phosphate buffer saline (PBS) and subsequently immersed in complete medium overnight before cell seeding. hFOB cells grown in 75 cm^2 cell culture flasks were detached by adding 1 mL of 0.25% trypsin containing 0.1% EDTA. Detached cells were centrifuged, counted by trypan blue assay using a hemocytometer and seeded on the scaffolds at a density of 7 x 10^3 cells/well and kept in incubator for facilitating cell growth, proliferation and mineralization. Cells seeded on tissue culture plate (TCP) were used as control to check the normal morphology and mineralization of cells compared to all other nanofibrous scaffolds.

hFOB Cells Proliferation

Cell proliferation was monitored after 5, 10, and 15 days of culture by MTS assay (3-(4,5-dimethylthiazol-2-yl)-5-(3-carboxymethoxyphenyl)-2-(4-sulfophenyl)-2H-tetrazolium, inner salt). In order to monitor cell adhesion and proliferation on different substrates, the number of cells was determined by using the colorimetric MTS assay (CellTiter 96® AQ_{ueous} Assay). The mechanism behind this assay is that, metabolically active cells react with a tetrazolium salt in MTS reagent to produce a soluble formazan dye that shows absorbance at 492 nm. The cellular constructs were rinsed with PBS followed by incubation with 20% MTS reagent in serum free medium for 3 h. Thereafter, aliquots were pipetted into 96-well plates and the samples read in a spectrophotometric plate reader at 492 nm (FLUOstar OPTIMA, BMG Lab Technologies, Germany).

Cell Morphology

Morphology and mineralization of the *in vitro* cultured hFOB cells on TCP, PCL, PCL\CQ, and PCL\CQ\HA were observed after 10 and 15 days of cell proliferation by processing the cell-cultured scaffolds for FESEM studies. The scaffolds were rinsed twice with PBS and fixed in 3% glutaraldehyde for 3 hrs. Thereafter, the scaffolds were rinsed in DI water and dehydrated with upgrading concentrations of ethanol (50%, 70% 90%, 100%) twice for 15 min each. Final washing with 100% ethanol was followed by treating the specimens with hexamethyldisilazane (HMDS). The HMDS was air-dried by keeping the samples in fume hood. Finally the scaffolds were sputter coated with gold and then observed under FESEM.

ALP Activity of hFOB Cells

ALP activity of hFOB was measured using alkaline phosphatase yellow liquid substrate system for ELISA (Sigma Life sciences, USA). The expression of alkaline phosphatase (ALP) activity of the cells shows bone forming ability of hFOB seeded on different scaffolds. In this reaction, ALP catalyzes the hydrolysis of colorless organic phosphate ester substrate, *p*-nitrophenylphosphate, to a yellow product, *p*-nitrophenol, and phosphate. Nanofibrous scaffolds with hFOBs were washed twice with PBS and incubated with 1 mL of ALP for 30 mins, further the reaction was stopped by using 2N NaOH. The yellow color product was aliquot in 96-well plate and read in spectrophotometric microplate reader and absorbance measured at 405 nm.

Mineralization of hFOB

Alizarin red-S (ARS) is a dye that binds selectively calcium salts and is widely used for calcium mineral histochemistry. ARS staining was used to detect and quantify mineralization. Nanofibrous scaffolds with hFOB cells (construct) were washed three times in PBS and fixed in ice-cold 70% ethanol for 1 h. These constructs were washed three times with dH_2O and stained with ARS (40 m*M*) for 20 min at room temperature. After several washes with dH_2O, these constructs were observed under optical microscope, and the stain was extracted with the use of 10% cetylpyridinium chloride for 1 h. The dye was collected and the absorbance was read at 540 nm in spectrophotometer (Thermo Spectronics, Waltham, MA).

Immunofluorescent Staining for Osteocalcin

Confocal studies were done for these scaffolds to identify the presence of bone specific protein in the scaffolds. Osteoblasts secreted proteins which help in identifying their functions and their level of mineralization. To analyse that, scaffolds were fixed in methanol and left in −20°C for 20 min. The scaffolds were then treated with 0.1% triton 100X for 1 min to permeabilize the cell walls to facilitate the migration and specific attachment of protein, and subsequent treatment with 3% BSA for one hour at room temperature. Osteocalcin was added as the primary antibody and left for one and half hour at room temperature then after PBS wash; it was treated with fluorescent tagged secondary antibody for another one and half hour then washed with PBS. Finally it was stained with DAPI for nucleus then the slides were mounted with the use of VECTA SHIELD.

Statistical Analysis

The data presented are expressed as mean ± standard deviation (SD). Statistical analysis was done using student's *t*-test and the significant level of the data was obtained. The $P \leq 0.05$ was considered to be statistically significant.

RESULTS AND DISCUSSION

Phytochemical Analysis

The active constituent phytosterols of *Cissus quadrangularis* are responsible for its osteoinductive property.[26] The preliminary phytochemical screening of the petroleum ether extract of *Cissus*

Figure 1. Image of *Cissus quadrangularis* herb showing 4-angled stems with fleshy 3-lobed leaves. Right top image shows phytochemical screening of the petroleum ether extracts of *Cissus quadrangularis* for phytosterols. Formation of brown ring (indicated by arrow) at the junction confirms the presence of phytosterols. [Color figure can be viewed in the online issue, which is available at wileyonlinelibrary.com.]

quadrangularis (Figure 1) shows the formation of brown ring at the junction which confirms the presence of phytosterols.

Characterization of Electrospun Fibers

FESEM micrographs of electrospun nanofibrous scaffolds of PCL, PCL-CQ, and PCL-CQ-HA revealed porous, beadless, nanoscaled fibrous structures formed under controlled conditions (Figure 2). PCL, PCL-CQ showed uniform smooth nanofibrous surface with diameter in the range of 519 ± 28, 161 ± 23 nm, respectively. In PCL-CQ-HA nanofibers, the HA nanoparticles were randomly distributed on the nanofiber surface which varies the fiber size tremendously with a mean fiber diameter of 303 ± 77 nm and imparting a rough texture to the scaffolds. The enhanced bioactivity and surface roughness provided by HA reinforcements may provide sites for protein adhesion, cell adhesion and proliferation. Surface roughness of nanofibrous scaffolds is desirable for better cell attachment and growth.[27] Hydrophilic nature is very important for the cell adhesion and proliferation. Especially for osteoblast cells the anchorage is very important. Contact angle helps to analyze the hydrophilic nature of the scaffolds. The contact angle of PCL scaffold is

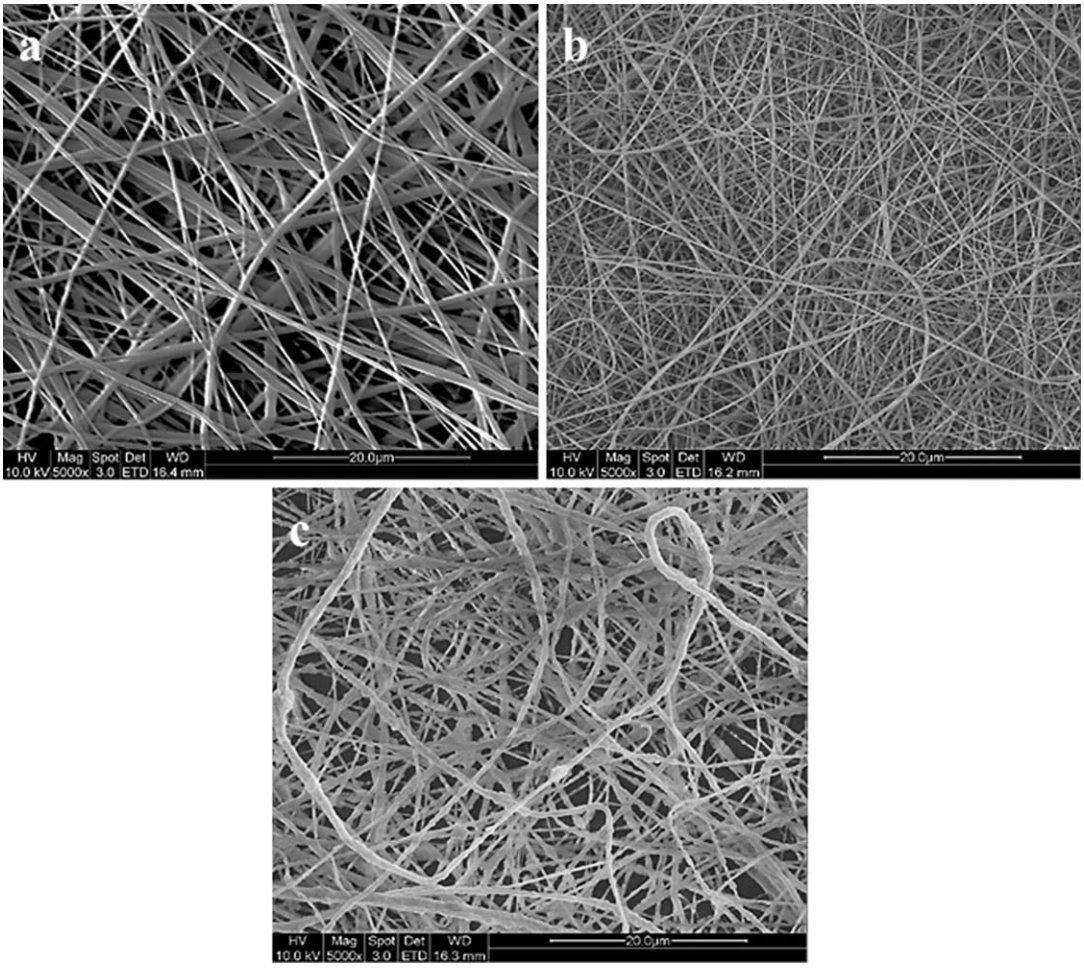

Figure 2. FESEM micrographs of (a) PCL, (b) PCL-CQ, and (c) PCL-CQ-HA nanofibrous scaffolds. PCL, PCL-CQ shows uniform smooth nanofibers whereas PCL-CQ-HA nanofiber shows rough texture due to randomly distributed HA nanoparticle on the nanofiber surface.

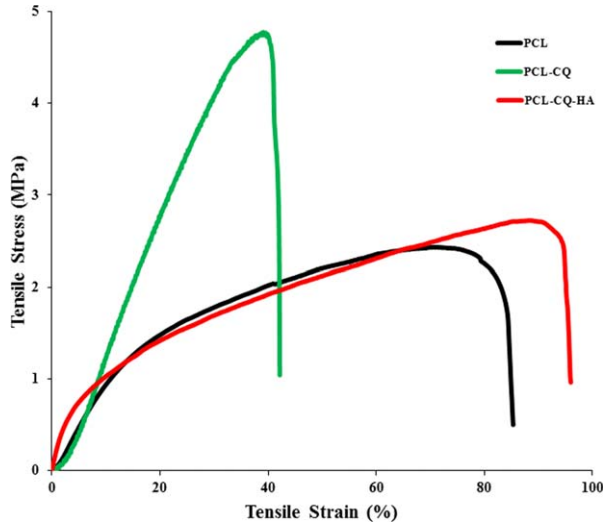

Figure 3. Tensile stress-strain curves of PCL, PCL-CQ, and PCL-CQ-HA nanofibrous scaffolds. HA incorporation increaseded rigidity of the scaffolds indicated by higher elastic modulus for PCL-CQ-HA nanfibrous scaffold suitable for bone related therapeutics. [Color figure can be viewed in the online issue, which is available at wileyonlinelibrary.com.]

133.30° because of its highly hydrophobic nature. The PCL-CQ nanofibrous scaffold has a contact angle of 37.40°. The presence of CQ has made the scaffold hydrophilic. The PCL-CQ-HA nanofibrous scaffold has a contact angle of around 58.20°, the rough surface and hydrophilic environment of the scaffold is expected to support better cell adhesion and proliferation. Tensile analysis helps to identify the capability of the scaffolds in hard tissue regeneration i.e. bone. Figure 3 shows the nonlinear stress strain graph of PCL, PCL-CQ and PCL-CQ-HA. The tensile stress, strain and elastic modulus of PCL, PCL-CQ, and PCL-CQ-HA are illustrated in Table I. Tensile stress at break for PCL, PCL-CQ, and PCL-CQ-HA were 0.79 MPa, 2.92 MPa, and 1.55 MPa and can bear a strain of 84%, 42%, and 95%, respectively. The Young's modulus value for PCL, PCL-CQ, and PCL-CQ-HA were 11.61 MPa, 12.66 MPa, and 29.48 MPa. The data showed blending of CQ and HA reduces the degree of close packing between caprolactone leaving the PCL-CQ and PCL-CQ-HA nanofibrous scaffold with better elastic properties. The observed 50% decrease in tensile properties for PCL-CQ compared to PCL may be due to increase in amorphous region in the blend and decreased intermolecular bonding. PCL-CQ-HA nanofibrous scaffolds showed increased tensile strain and modulus which may be due to HA incorporation which increased the rigidity of the scaffolds, similar results were obtained where HA reinforcement increases the compressive modulus of collagen matrix.[28] The mechanical strength proved that PCL-CQ-HA nanofibrous scaffolds have better elastic modulus compared to other scaffolds which is very important for clinically useful scaffolds that retain their shape during implantation and ideally bear mechanical loads after implantation especially for bone tissue engineering.

Table I. Characterization of Electrospun Nanofibers for Fiber Diameter, Water Contact Angle, and Mechanical Properties

Nanofiber construct	Fiber diameter (nm)	Water contact angle (°)	Tensile strength (MPa)	Tensile Break (%)	Young's modulus (MPa)
PCL	519 ± 28	133.30	0.79	84	11.61
PCL-CQ	161 ± 23	37.40	2.92	42	12.66
PCL-CQ-HA	303 ± 77	58.20	1.55	95	29.48

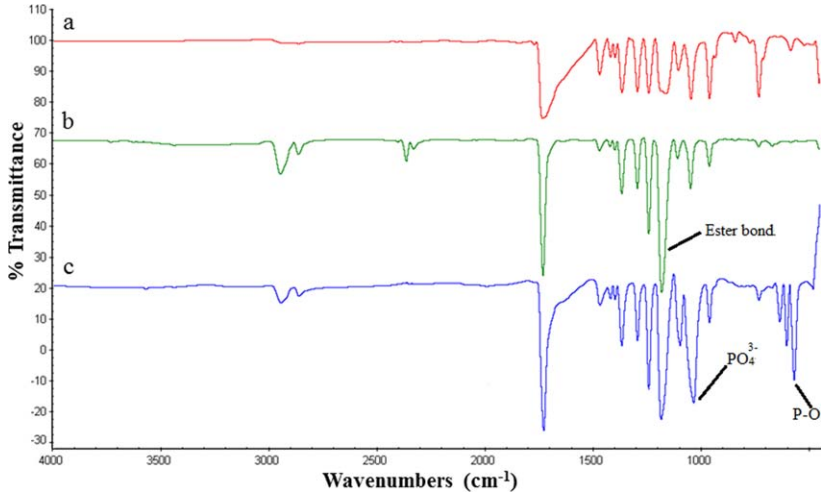

Figure 4. FTIR spectroscopic analysis of (a) PCL, (b) PCL-CQ, and (c) PCL-CQ-HA nanofibrous scaffolds showing characteristic peaks of PCL, CQ, and HA confirming their successful blending in nanofibrous scaffolds. [Color figure can be viewed in the online issue, which is available at wileyonlinelibrary.com.]

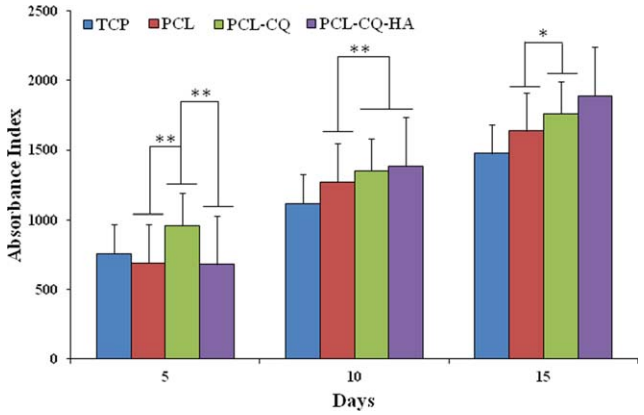

Figure 5. Cell proliferation study of hFOB cells on TCP, PCL, PCL-CQ, and PCL-CQ-HA nanofibrous scaffolds on Days 5, 10, and 15. * indicates significant difference of $P \leq 0.05$; ** indicates significant difference of $P \leq 0.01$. [Color figure can be viewed in the online issue, which is available at wileyonlinelibrary.com.]

FTIR spectra of PCL, PCL-CQ, and PCL-CQ-HA nanofibrous scaffolds (Figure 4) were compared. The characteristics peaks of PCL namely C═O vibration at 1728 cm^{-1}, CH_2 band vibrations at 1362, 1407, and 1465 cm^{-1}, esteric COO vibrations at 1181 and 1238 cm^{-1}, O—C vibrations at 1099, 1047, and 961 cm^{-1}, CH_2 rocking vibration occurring at 729 cm^{-1} are clearly seen in the spectrum [Figure 4(a)]. The FTIR spectrum of CQ loaded PCL is shown in spectrum [Figure 4(b)]. The bands correspond to C—H and C═O stretching is seen at 1722 cm^{-1} and 1454 cm^{-1} respectively, C═C stretching vibration of aromatic occurs at 1638 cm^{-1}. C—N stretching of amines is observed from 1000 to 1150 cm^{-1} and these corresponds to the C—N stretching in aliphatic amines, amide III and amide I bands of proteins and carbonyl groups respectively. The band positions from 645 to 686 are due to C—C and C—H phenyl ring substitution. These IR bands observed correspond to the flavonoids and terpenoids as expected for this plant. The FTIR spectrum of PCL-CQ-HA is shown in spectrum [Figure 4(c)]. It carries the features of both the spectrum of PCL and PCL-CQ nanofibrous scaffolds. Additionally stretching vibration for PO_4^{3-} group from mineral HA were obtained at 1053 cm^{-1} for P—O stretch and at 573 cm^{-1} for P—O stretch coupled with P—O bend, bands pertaining to CO_3^{2-} group from carbonate substituted OH and PO_4^{3-} groups in HA were obtained at about 1400 cm^{-1}, in the HA containing scaffolds, which is similar to that

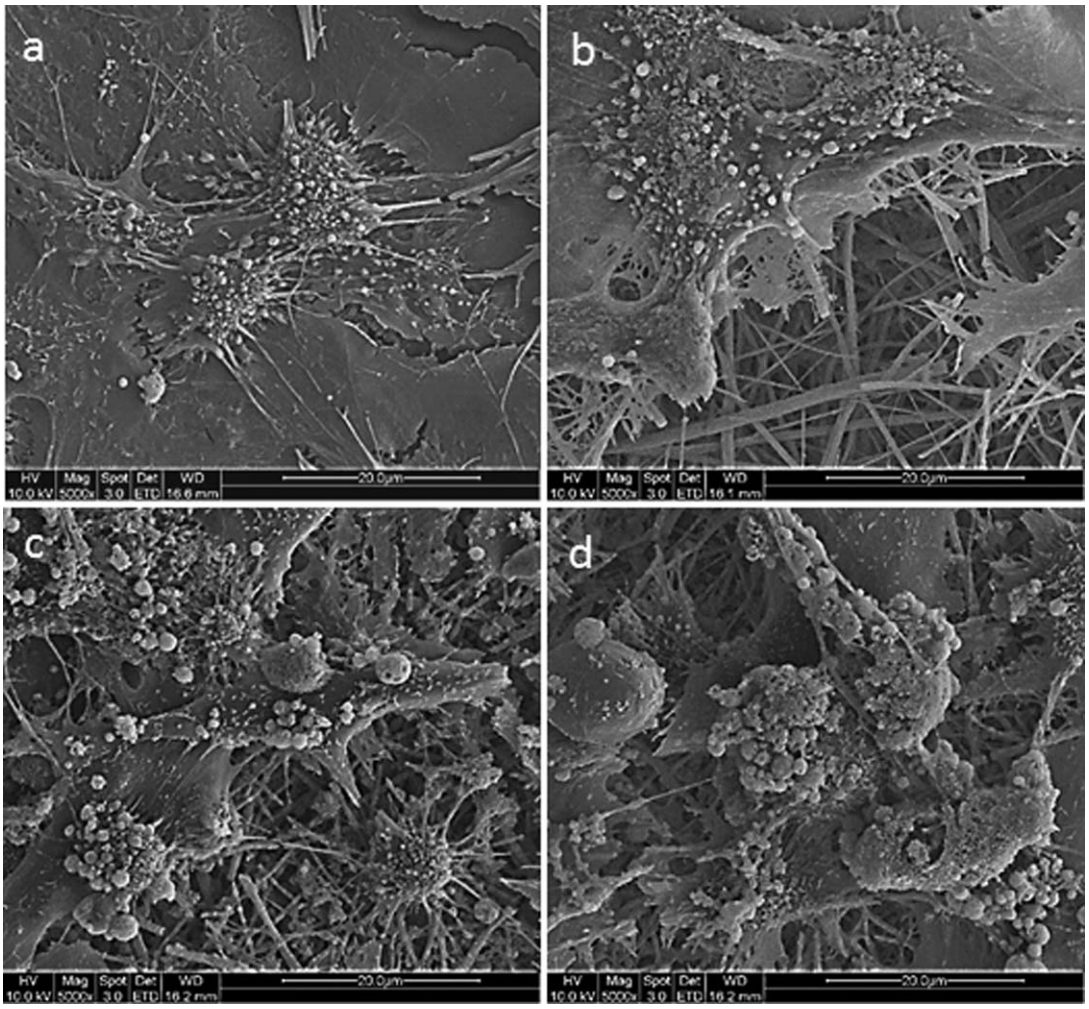

Figure 6. FESEM images showing the cell-biomaterial interactions on Day 10 on (a) TCP, (b) PCL, (c) PCL-CQ, and (d) PCL-CQ-HA nanofibrous scaffolds at 5000x magnification.

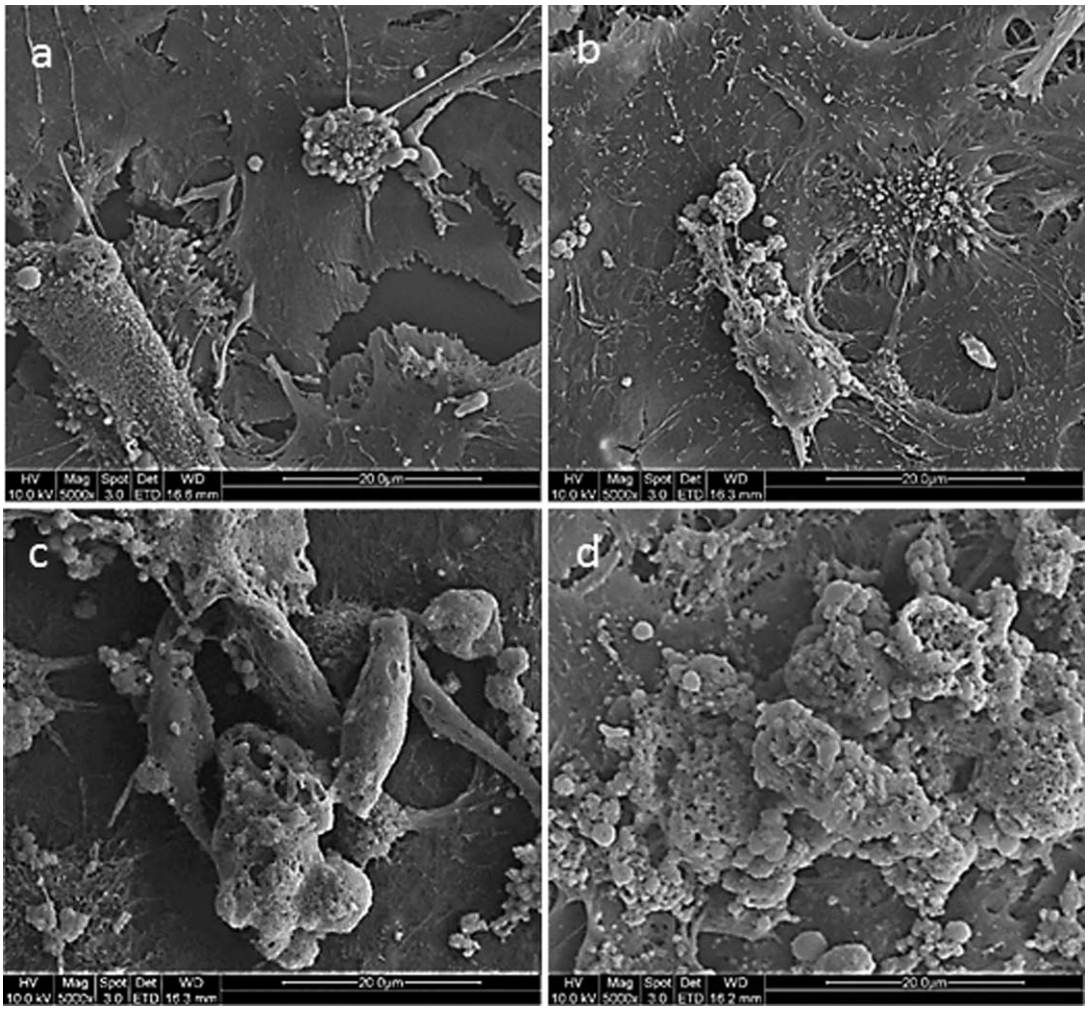

Figure 7. FESEM images showing the cell-biomaterial interactions on Day 15 on (a) TCP, (b) PCL, (c) PCL-CQ, and (d) PCL-CQ-HA nanofibrous scaffolds at 5000x magnification. Higher level of mineralization observed on the surface of PCL-CQ and PCL-CQ-HA nanofibrous scaffolds forming a thick layer along with ECM production by cells.

found in bone, thus confirming bone like chemical composition and expected to have better cell proliferation and mineralization on this scaffolds for bone tissue engineering.

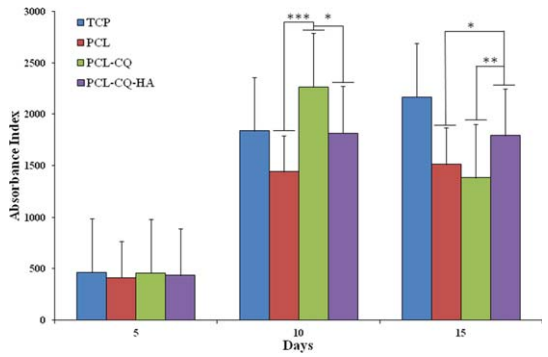

Figure 8. Alkaline phosphatase activity of hFOB on TCP, PCL, PCL-CQ, and PCL-CQ-HA nanofibrous scaffolds on Days 5, 10, and 15. * indicates significant difference of $P \leq 0.05$; ** indicates significant difference of $P \leq 0.01$ and *** indicates significant difference of $P \leq 0.001$. [Color figure can be viewed in the online issue, which is available at wileyonlinelibrary.com.]

Interaction of Cells and Scaffolds

The hFOB cultured on TCP, PCL, PCL-CQ, PCL-CQ-HA nanofibrous scaffolds and monitored for cell proliferation after 5, 10, and 15 days of cell seeding are shown in Figure 5. PCL-CQ increases cell proliferation significantly ($P \leq 0.01$) on Day 5 about 39% and 41% compared to PCL and PCL-CQ-HA proving CQ to be osteogenic properties. However the cell proliferation on PCL-CQ-HA nanofibrous scaffolds showed significant increase on Days 10 and 15 than the other scaffolds because of the rough surface morphology of the scaffold which supported the cell adhesion and proliferation for longer period of time. PCL-CQ-HA proves to be a potential scaffold for bone tissue regeneration. Cell morphology and mineralization of hFOB cultured on different scaffolds on Days 10 and 15 were observed by FESEM. The FESEM images of hFOB revealed normal cuboidal osteoblast-like morphology were observed on PCL-CQ, PCL-CQ-HA nanofibrous scaffolds (Figures 6 and 7). Cells presented typical osteoblast phenotypes: attaching to the polymers with filapodia, and bridging each other with extracellular matrix they synthesized and calcified with the formation of mineral particles on the surface of the cells after Day 10 of cell culture.

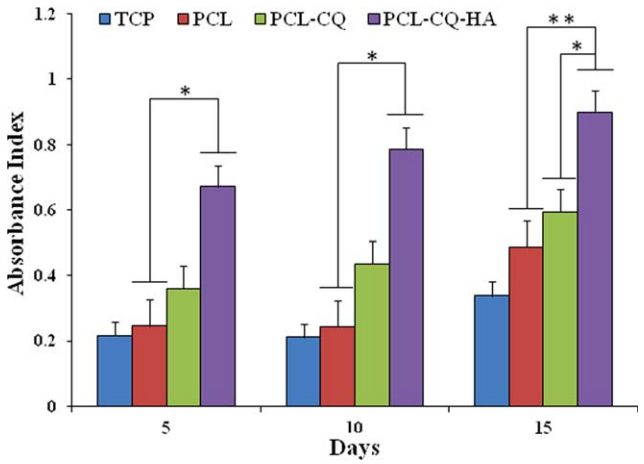

Figure 9. Quantitative analysis for the mineralization of hFOB on TCP, PCL, PCL-CQ, and PCL-CQ-HA nanofibrous scaffolds on Days 5, 10, and 15. * indicates significant difference of $P \leq 0.01$; ** indicates significant difference of $P \leq 0.001$. [Color figure can be viewed in the online issue, which is available at wileyonlinelibrary.com.]

After Day 15 of culture, increased level of mineralization were observed on PCL-CQ and PCL-CQ-HA but comparatively higher with fused cells forming a thick layer on the surface of the scaffolds along with ECM production by cells. HA acts as a chelating agent for the mineralization of osteoblasts for bone tissue regeneration.

Mineralization and Osteocalcin Expression of Osteogenic Cells

ALP has a crucial role for the initiation of mineralization process; it hydrolyses phosphate esters and increases the local phosphate concentration, further enhancing the mineralization of ECM.[29] ALP activity of hFOB cultured on TCP, PCL, PCL-CQ, and PCL-CQ-HA scaffolds monitored after 5, 10, and 15 days of cell seeding are shown in Figure 8. Results of the ALP activity of hFOB cultured was almost equal on all the scaffolds on Day 5 with no significant differences. However PCL-CQ and PCL-CQ-HA nanofibrous scaffold showed significant increase of ($P \leq 0.001$) 57.41% and ($P \leq 0.05$) 26.11% in ALP activity on Day 10 compared to PCL scaffold proving CQ enhances ALP

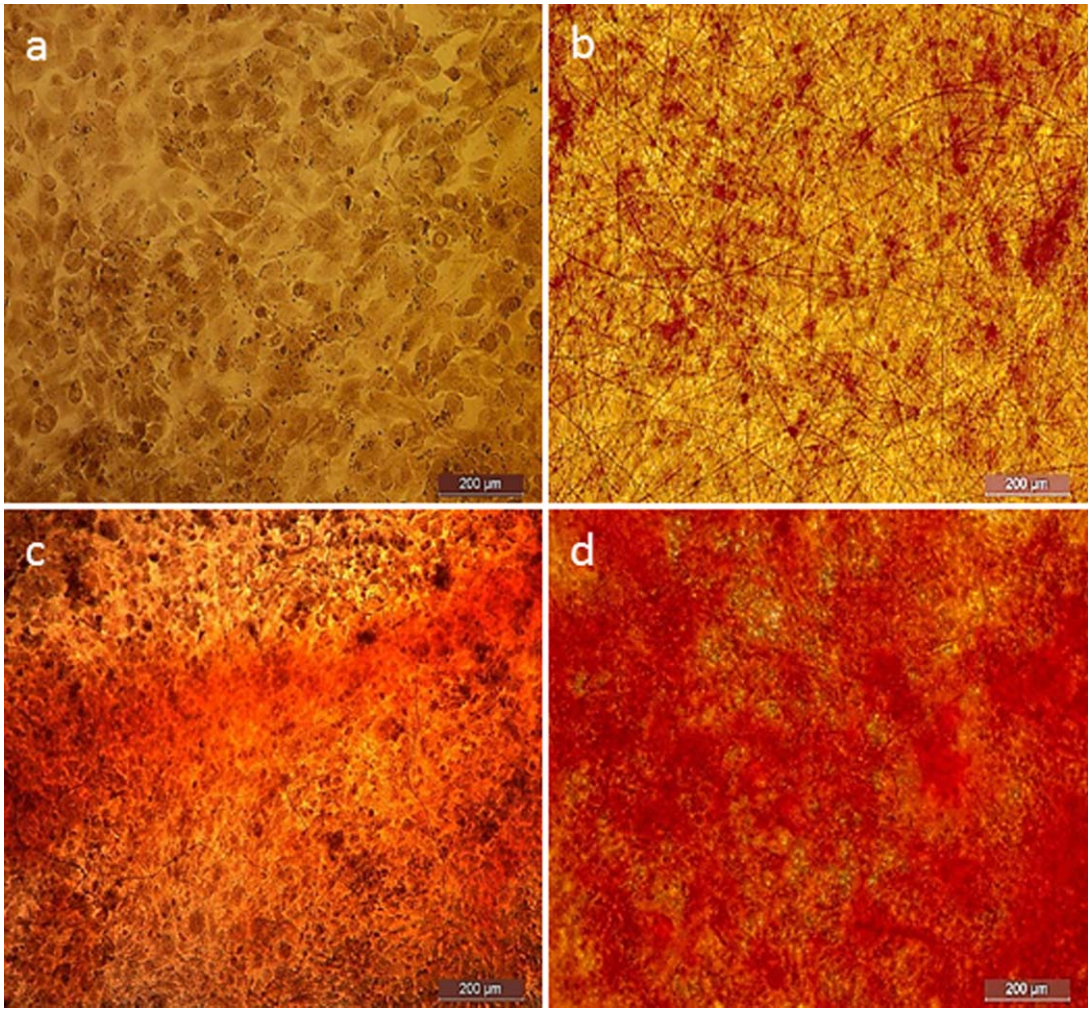

Figure 10. Optical microscope images showing the secretion of extracellular matrix by hFOB using Alizarin red staining on Day 10 on (a) TCP, (b) PCL, (c), PCL-CQ, and (d) PCL-CQ-HA nanofibrous scaffolds at 10x magnification. Both PCL-CQ and PCL-CQ-HA showed significant increase in calcium deposition compared to TCP and PCL nanofibrous scaffold. [Color figure can be viewed in the online issue, which is available at wileyonlinelibrary.com.]

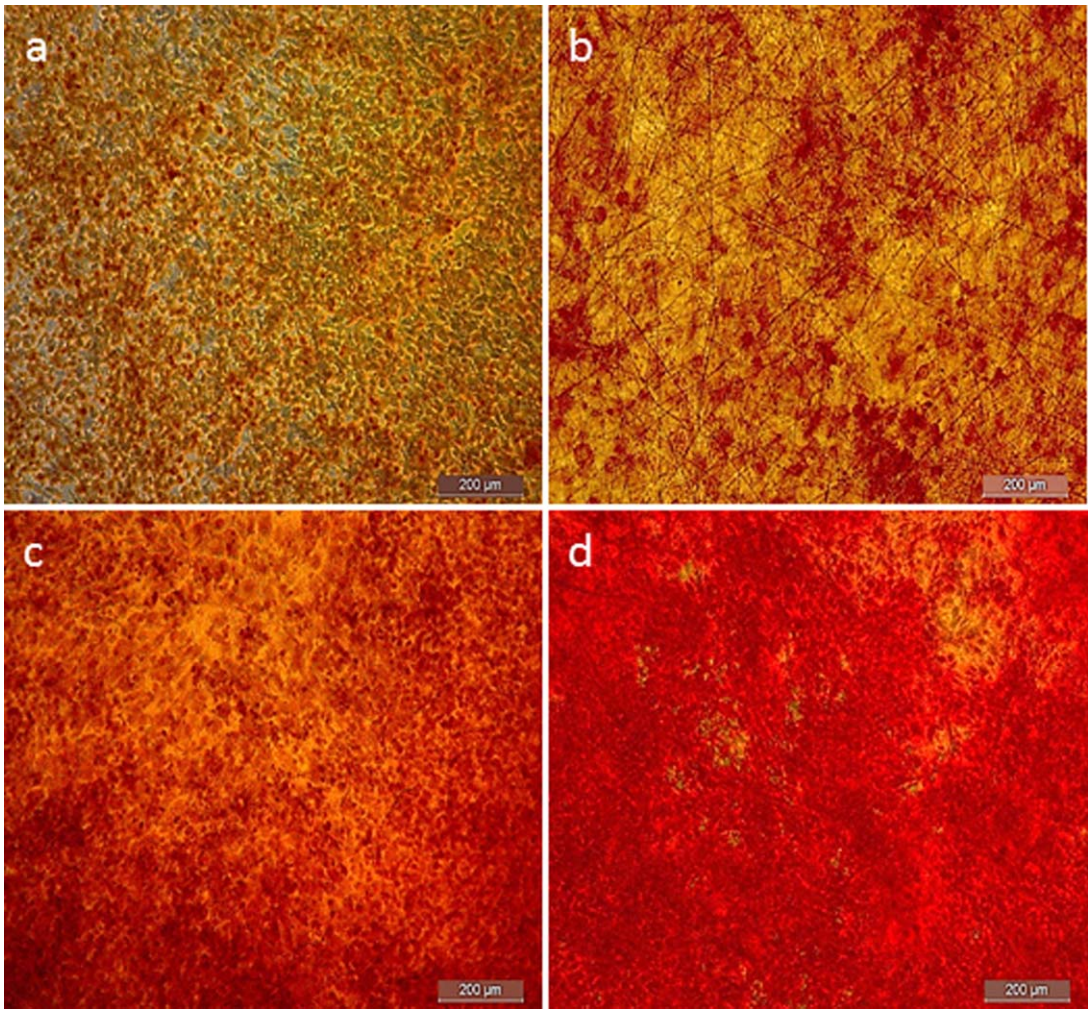

Figure 11. Optical microscope images showing the secretion of extracellular matrix by hFOB using Alizarin red staining on Day 15 on (a) TCP, (b) PCL, (c) PCL-CQ, and (d) PCL-CQ-HA nanofibrous scaffolds at 10x magnification. PCL-CQ-HA scaffolds showed significant increase in calcium deposition compared to TCP and other nanofibrous scaffolds. [Color figure can be viewed in the online issue, which is available at wileyonlinelibrary.com.]

activity. On Day 15 PCL-CQ-HA showed prolonged increase in ALP activity about ($P \leq 0.05$) 29.67% and ($P \leq 0.01$) 18.45% compared with PCL-CQ and PCL scaffolds. ALP activity on Day 15 was comparatively less than Day 10 for PCL, PCL-CQ, and PCL-CQ-HA scaffolds that may probably due to the increase of bone mineralization. The results showed that significant level of synergistic effect of HA and CQ in bone tissue regeneration. ARS staining was used to characterize the bone nodule formation of hFOB cultured on different electrospun nanofibers. The results of the quantitative analysis of the minerals deposited on TCP, PCL, PCL-CQ, and PCL-CQ-HA nanofibrous scaffolds were shown in Figure 9. The measured absorbance from PCL-CQ-HA scaffolds was significantly ($P \leq 0.01$) higher on Days 5 and 10 and about 84.60% ($P \leq 0.001$) higher than the PCL on 15 days. Both PCL-CQ and PCL-CQ-HA showed no significance difference on Days 5 and 10 however the mineralization on PCL-CQ-HA nanofibrous scaffold was increased about 50% ($P \leq 0.01$) on Day 15. Optical microscopic images in Figures 10 and 11 of scaffolds with ARS staining after 10 and 15 days of cell culture supported the above data where high intensity of minerals stained was observed on PCL-CQ-HA nanofibrous scaffolds, typical of their calcium deposition than the other scaffolds proving it to be the superior scaffold for bone tissue engineering. Osteocalcin is secreted solely by osteoblasts and it plays a vital role in bone metabolic regulation and bone building by nature.[30] The presence of osteocalcin signifies the possible bone formation which is a positive step towards bone regeneration technique. High osteocalcin levels are correlated with the increase in bone mineral density (BMD). So the presence of osteocalcin in a particular scaffold explains the scaffolds suitability for the use in bone formation/regeneration process. Confocal images of the osteoblast cells expressing osteocalcin protein on TCP, PCL, PCL-CQ, and PCL-CQ-HA were given in Figure 12. Osteobalst cells showed even distribution on PCL-CQ-HA nanofibrous scaffolds and maintained phenotypic expression for this bone specific protein in higher level which proves it as a suitable scaffold for bone tissue regeneration.

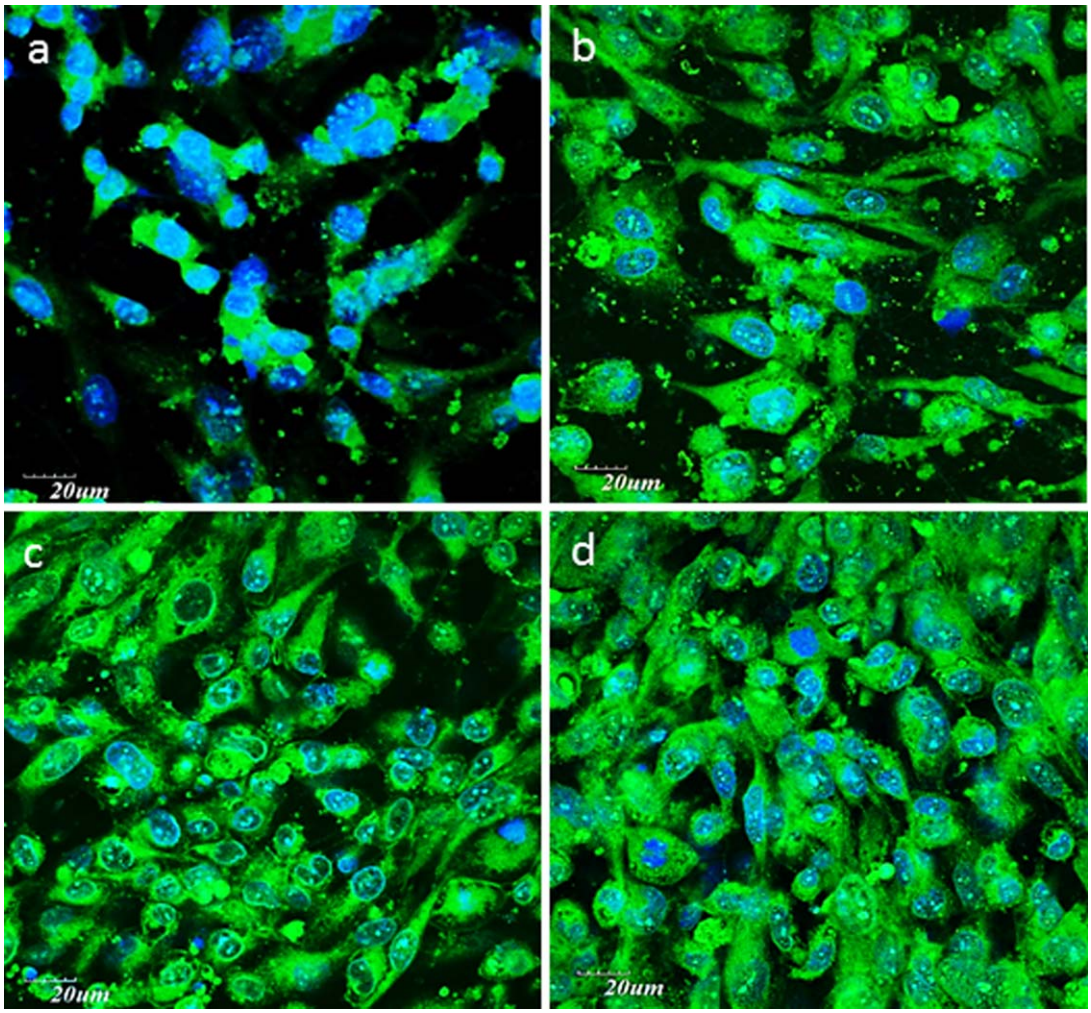

Figure 12. Confocal microscopy images showing osteoblasts specific marker protein osteocalcin expression of hFOB cells on (a) TCP, (b) PCL, (c) PCL-CQ, and (d) PCL-CQ-HA nanofibrous scaffolds at 60x magnification. The protein was labelled with FITC (green) and nucleus with DAPI (blue). [Color figure can be viewed in the online issue, which is available at wileyonlinelibrary.com.]

CONCLUSIONS

The essential constituents for successful tissue engineering include biocompatible scaffolds with bioactive molecules stimulating proliferation and regeneration following implantation into the defect site of the host. To facilitate cell adhesion and proliferation, high surface area and interconnected pore structure are desirable. The fabrication of herbal scaffolding approach for bone tissue engineering applications by incorporating CQ and HA with PCL nanofibrous scaffold to enhance the favorable environment for osteoblast response and enhanced secretion of mineralization for bone formation. Physicochemical property of the developed nanofibrous scaffold also proves it to be an efficient tissue scaffold. The CQ-loaded nanofibers retained its biological functionality even after it had been subjected to a high electrical voltage. The observed results indicate that both PCL-CQ and PCL-CQ-HA enhanced osteoblast proliferation and mineralization however PCL-CQ-HA responses to cellular interaction was much more notable proving CQ in combination with HA will be a promising approach for solving the current issues related to bone defects.

ACKNOWLEDGMENTS

This work was supported by The Department of Textile Technology, Anna University Chennai, India, NRF-Technion and NUSNNI, National University of Singapore, Singapore.

REFERENCES

1. Lalan, S.; Pomerantseva, I.; Vacanti, J. P. *World J. Surg.* **2001**, *25*, 1458.
2. Langer, R.; Vacanti, J. P. *Science* **1993**, *260*, 920.
3. Chan, B. P.; Leong, K. W. *Eur. Spine J.* **2008**, *17*, 467.
4. Venugopal, J.; Ramakrishna, S. *Tissue Eng.* **2005**, *11*, 847.
5. Venugopal, J.; Ramakrishna, S. *Appl. Biochem. Biotech.* **2005**, *125*, 147.
6. Sabir, M. I.; Xu, X.; Li, L. *J. Mater. Sci.* **2009**, *44*, 5713.
7. Laurencin, C. T.; Ambrosio, A. M. A.; Borden, M. D.; Cooper, J. A. *Biomed. Eng.* **1999**, *1*, 19.
8. Ma, P. X.; Zhang, R. J. *J. Biomed. Mater. Res.* **1999**, *46*, 60.

9. Fertala, J.; Han, W. B.; Ko, F. K. *J. Biomed. Mater. Res.* **2001**, *57*, 48.
10. Li, W. J.; Laurencin, C. T.; Caterson, E. J.; Tuan, R. S.; Ko, F. K. *J. Biomed. Mater. Res.* **2002**, *60*, 613.
11. Luu, Y. K.; Kim, K.; Hsiao, B. S.; Chu, B.; Hadjiargyrou, M. *J. Control Release* **2003**, *89*, 341.
12. Suganya, S.; Senthil Ram, T.; Lakshmi, B. S.; Giridev, V. R. *J. Appl. Polym. Sci.* **2011**, *121*, 2893.
13. Yoshimoto, H.; Shin, Y. M.; Terai, H.; Vacanti, J. P. *Biomaterials* **2003**, *24*, 2077.
14. Venugopal, J.; Rajeswari, R.; Shayanti, M.; Low, S.; Bongso, A.; Giri Dev, V. R.; Deepika, G.; Ramakrishna, S. *J. Biomater. Sci. Polym. Ed.*, **2013**, *24*, 170.
15. Garima, M.; Saurabh, S.; Nagori, B. P. *Int. J. Pharm. Tech. Res.* **2010**, *2*, 1298.
16. Jakikasem, S.; Limsiriwong, P.; Kajsongkarm, T.; Sontorntanasart, T. *Thai. J. Pharm Sci.* **2000**, *24*, 25.
17. Chopra, S. S.; Patel, M. R.; Gupta, L. P.; Datta, I. C. *Indian J. Med. Res.* **1975**, *63*, 824.
18. Udupa, K. N.; Prasad, G. C. *Indian J. Med. Res.* **1964**, *52*, 480.
19. Madan, N. *J. Sci. Ind. Res.* **1953**, *18*, 253.
20. Sen, S. P. *J. Me.d Res.* **1963**, *4*, 26.
21. Mehta, M.; Kaur, N.; Bhutani, K. K. *Phytochem. Analysis* **2001**, *12*, 91.
22. Potu, B. K.; Rao, M. S.; Kutty, G. N.; Bhat, M. R. K.; Chamallamudi, M. R.; Nayak, S. R. *Clin. Sci.* **2008**, *63*, 815.
23. Shirwaiker, A.; Khan, S.; Malini, S. *J. Ethnopharmacol.* **2003**, *89*, 245.
24. Fabre, T.; Schappacher, M.; Bareille, R.; Dupty, B.; Soum, A.; Bertrand-Barat, J.; Baquey, C. *Biomaterials* **2001**, *22*, 2951.
25. Jin, W. J.; Lee, H. K.; Jeong, E. H.; Park, W. H.; Youk, J. H. *Macromol. Rapid. Commun.* **2005**, *26*, 1903.
26. Sudha, S. R.; Murugesan, M. *Int. J. Pharm. Pharm. Sci.* **2012**, *4*, 975.
27. Rui, F.; Enwei, Z.; Ling, X.; Shicheng, W. *J. Nanosci. Nanotechnol.* **2010**, *10*, 7747.
28. Kane, R. J.; Roeder, R. K. *J. Mech. Behav. Biomed.* **2012**, *7*, 41.
29. Bellows, C. G.; Aubin, J. E.; Heersche, J. N. *Bone. Miner.* **1991**, *14*, 27.
30. Lee, N. K.; Sowa, H.; Hinoi, E.; Ferron, M.; Ahn, J. D.; Confavreux, C.; Dacquin, R.; Mee, P. J.; McKee, M. D.; Jung, D. Y.; Zhang, Z.; Kim, J. K.; Mauvais-Jarvis, F.; Ducy, P.; Karsenty, G. *Cell* **2007**, *130*, 456.